Fast algorithm for quadratic aberration model based on cross triple correlation

Wei Liu [a], Tingting Zhou [a], Shiyuan Liu *[b]

[a] Wuhan National Laboratory for Optoelectronics, Huazhong University of Science and Technology, Wuhan, China;
[b] State Key Laboratory of Digital Manufacturing Equipment and Technology, Huazhong University of Science and Technology, Wuhan, China.

ABSTRACT

The quadratic aberration model used in optical lithography is a natural extension of the linear model by taking into account interactions among individual Zernike coefficients. Although the model has been tested and verified in many applications, the effects of Zernike coefficients under partially coherent imaging are usually obtained by extensive experiments due to complexity of the model expression. In this paper, a generalized cross triple correlation (CTC) is introduced, and a fast algorithm to simulate the quadratic aberration model is developed. Simulations were performed by the proposed CTC based algorithm with different input Zernike aberrations for binary and phase shift masks with multiple pitches and orientations, which demonstrate that the proposed approach is not only accurate but also efficient for revealing the influence of different Zernike orders on aerial image intensity distributions under partially coherent illumination.

Keywords: wavefront aberration, quadratic aberration model, cross triple correlation (CTC), transmission cross coefficient (TCC), partial coherent imaging, optical lithography

1. INTRODUCTION

As the limit of optical lithography is pushed and feature densities continue to increase, lens aberration has become one of the most important factors to evaluate the imaging quality of lithographic tools [1-3]. One method to mathematically model lens aberrations utilizes Zernike polynomials, which are a complete orthogonal set of polynomials over the interior of the unit circle [4,5]. The Zernike series representation is useful as it provides explicit expressions for the well-known aberrations such as spherical, coma, astigmatism, etc., which can be classified into odd aberrations and even aberrations. Odd aberrations cause the image displacement and line-width asymmetry that influence the critical dimension uniformity [6], together with even aberrations reducing the maximum image irradiance and image log-slope which affects usable depth of focus [7]. Moreover, the interaction among different types of aberrations brings about the distinct deterioration of intensity or relative parameters such as critical dimension (CD) uniformity and position shift [8]. Considering the multiplicity of the Zernike aberration in practical projection lens, a detailed understanding and evaluating the effects of wavefront aberration represented by Zernike coefficients on imaging is crucial in lithography.

The imaging optics configuration in lithographic tools is typically a partially coherent system that is characterized by the intensity distribution of the effective source and the pupil function of the projection lens. Imaging properties of such partially coherent systems have to be described using a bilinear model [9], which leads to time-consuming calculations and understanding difficulties, especially in the case when the wavefront aberration is involved. Recent years, an approximate linear response model of Zernike coefficients to the aerial image displacement has been reported and widely utilized for aberration comprehension and measurement. The linear relationship can be established between the intensity difference of adjacent peaks in the one-dimensional binary gating images [6,7,10], by supposing that the individual Zernike aberration in current lithographic projection lens is very small. Although this linear response model has a wide real-world application of Zernike aberration characterization based on one-dimensional masks, it is needed to develop a more generalized Zernike response model suitable not only for one-dimensional but also for two-dimensional masks with a

* Contact author: shyliu@mail.hust.edu.cn; phone: +86 27 87792409; fax: +86 27 87792413; http://www2.hust.edu.cn/nom.

Optical Microlithography XXIV, edited by Mircea V. Dusa, Proc. of SPIE Vol. 7973,
79731M · © 2011 SPIE · CCC code: 0277-786X/11/$18 · doi: 10.1117/12.879217

relatively large amount of individual Zernike aberration. A quadratic aberration model which is a natural extension of the linear response model has been reported by taking into account interactions among individual Zernike aberrations [11]. The quadratic aberration model has been tested and verified in many applications under both one-dimensional and two-dimensional masks, such as CD uniformity [8], aberration sensitivity analysis [12], and phase wheel target aberration monitoring [13]. However, the effects of Zernike aberrations on partially coherent imaging are usually obtained by extensive experiments or lithographic simulators [14], due to the complexity of the model formulation. The calculation of the quadratic aberration model directly by analytical expression is time consuming and thus impractical for in-situ measurement or characterization.

In this paper, a generalized cross triple correlation (CTC) is introduced for fast calculating the quadratic aberration model. By decomposition of the transition cross coefficient (TCC) into CTCs, the Zernike aberration-induced intensities in the quadratic aberration model can be calculated quickly and separated clearly from each other. Simulations were performed by the proposed CTC based algorithm with different input Zernike aberrations for binary and phase shift masks with multiple pitches and orientations, which demonstrates that the proposed approach is not only accurate but also efficient for revealing the influence of different Zernike orders on aerial image intensity distributions under partially coherent illumination. It is expected that this method will have applications in the robust optical proximity correction (OPC) and inverse mask design with aberrations taking into account. It will also have applications in the aerial image based aberration analysis and metrology.

2. THEORY

2.1 Optical imaging system

An optical lithography imaging system is shown in Fig. 1, in which both the object and the light source are of finite extent. In order to simplify the expressions of the imaging system, in the drawing we introduce the Cartesian object plane coordinates $\mathbf{x_0}$, image plane coordinates $\mathbf{x}$ and pupil plane coordinates $\mathbf{f}$, which are two-dimensional real vectors and all normalized according to canonical coordinates proposed by Hopkins [2], thus the cut off frequency from the pupil plane is normalized to the unit of one. The scalar form of Hopkins imaging theory for partially coherent imaging is used to depict its behavior [15]:

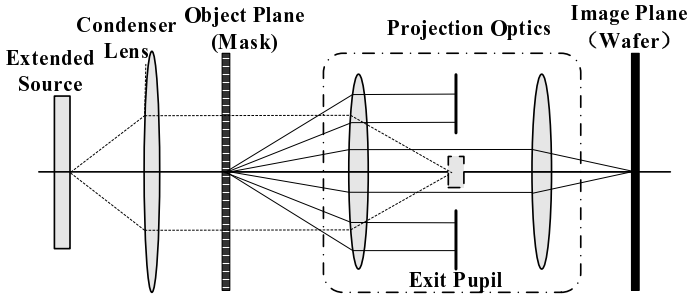

Fig. 1. Optical lithography imaging system.

$$I(\mathbf{x}) = \iint O(\mathbf{f}_1) O^*(\mathbf{f}_2)\, \mathrm{TCC}(\mathbf{f}_1, \mathbf{f}_2) \exp\left[-2\pi i(\mathbf{f}_1 - \mathbf{f}_2)\cdot \mathbf{x}\right] d\mathbf{f}_1 d\mathbf{f}_2, , \tag{1}$$

where TCC($\mathbf{f}_1$, $\mathbf{f}_2$) is introduced as the concept of the transmission cross coefficient:

$$\mathrm{TCC}(\mathbf{f}_1, \mathbf{f}_2) = \int J(\mathbf{f}) H(\mathbf{f} + \mathbf{f}_1) H^*(\mathbf{f} + \mathbf{f}_2) d\mathbf{f}. \tag{2}$$

Here $O(\mathbf{f})$ is the diffraction spectrum of a mask pattern. $J(\mathbf{f})$ describes the effective source intensity distribution under Kohler illumination. With a conventional circular illumination, it is constant within a radius proportional to partial coherence factor (σ):

$$J(\mathbf{f}) = \frac{1}{\pi\sigma^2} \mathrm{circ}\left(\frac{|\mathbf{f}|}{\sigma}\right). \tag{3}$$

$H(\mathbf{f})$ is the objective pupil function and is given by

$$H(\mathbf{f}) = \exp\left[-ikW(\mathbf{f})\right], \tag{4}$$

where k=2π/λ is the wave number, λ is the wavelength of the monochromatic light source, and $W(\mathbf{f})$ is the total aberrated wavefront including the lens aberration $W_{\text{lens}}(\mathbf{f})$ and an even-type aberration $W_{\text{defocus}}(\mathbf{f})$ that is induced by and proportional to the axial shift h (in nm) of the image plane:

$$W(\mathbf{f}) = W_{lens}(\mathbf{f}) + W_{defocus}(\mathbf{f}), \tag{5}$$

$$W_{defocus}(\mathbf{f}) = h \cdot w_{defocus}(\mathbf{f}) = h\left[\sqrt{1 - NA^2\left|\mathbf{f}\right|^2} - 1\right], \tag{6}$$

where NA is the image-side numerical aperture of the projection lens. The lens aberration function can be can be expressed as orthonormal Zernike fringe polynomials:

$$W_{lens}(\mathbf{f}) = \sum_n Z_n R_n(\mathbf{f}), \tag{7}$$

where n indicates Zernike index, $R_n(\mathbf{f})$ indicates the n^{th} Zernike polynomial for normalized Cartesian coordinate over the pupil plane.

2.2 Theory and algorithm of CTC

The cross triple correlation (CTC) is defined as [16]:

$$C_{KLM}(\mathbf{f}_1, \mathbf{f}_2) = \int K(\mathbf{f}) L(\mathbf{f} + \mathbf{f}_1) M(\mathbf{f} + \mathbf{f}_2) d\mathbf{f}, \tag{8}$$

where $K(\mathbf{f})$, $L(\mathbf{f})$, and $M(\mathbf{f})$ are three different functions. $\mathbf{f}$, $\mathbf{f}_1$, and $\mathbf{f}_2$ are variables that can be any real scalars for a one-dimensional signal, or two-dimensional real vectors representing the normalized spatial-frequency pupil coordinates. Most of the physical functions required for analysis of lithographic systems have compact support, and integration can be treated over whole space of $\mathbf{f}$. It is interesting to note that the expression of TCC in Eq. (2) is quite similar to the CTC in Eq. (8), except with the difference that the last two functions involved in TCC are two conjugate pupils instead of the two fully independent functions in CTC. Therefore, TCC can be considered as a special case of CTC.

From Eq. (8), each point in $C_{KLM}(\mathbf{f}_1,\mathbf{f}_2)$ is the integral area of the product of three functions when two movable ones are on a specific position as shown in Fig. 2. Especially, as $\mathbf{f}$, $\mathbf{f}_1$, and $\mathbf{f}_2$ are two-dimensional real vectors, the $C_{KLM}(\mathbf{f}_1,\mathbf{f}_2)$ becomes a four-dimensional matrix. It is time consuming to obtain each point in the four-dimensional matrix directly by Eq. (8), because of repeating integrations are needed for different positions $(\mathbf{f}_1,\mathbf{f}_2)$.

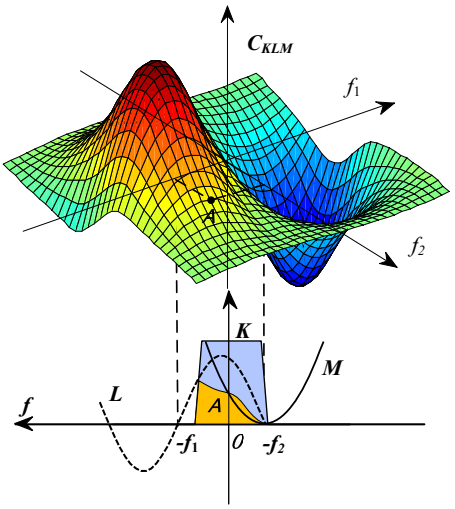

Fig. 2. Representation of the mathematical meaning of CTC.

To achieve an efficient CTC calculation, in this paper we utilize the fast Fourier transform (FFT) based algorithm. Let $c_{klm}(\mathbf{x}_1,\mathbf{x}_2)$, $k(\mathbf{x}_1,\mathbf{x}_2)$, $l(\mathbf{x}_1,\mathbf{x}_2)$ and $m(\mathbf{x}_1,\mathbf{x}_2)$ are the Fourier transform of $C_{KLM}(\mathbf{f}_1,\mathbf{f}_2)$, $K(\mathbf{f}_1,\mathbf{f}_2)$, $L(\mathbf{f}_1,\mathbf{f}_2)$ and $M(\mathbf{f}_1,\mathbf{f}_2)$,

respectively. Based on the theorem of Tichmarch, the cross triple correlation (CTC) can be treated as a kind of generalized convolution, and then the $c_{klm}(\mathbf{x}_1,\mathbf{x}_2)$, $k(\mathbf{x}_1,\mathbf{x}_2)$, $l(\mathbf{x}_1,\mathbf{x}_2)$ and $m(\mathbf{x}_1,\mathbf{x}_2)$ satisfy [16]:

$$c_{klm}(\mathbf{x}_1,\mathbf{x}_2) = k(\mathbf{x}_1)l(\mathbf{x}_2)m(-\mathbf{x}_1-\mathbf{x}_2). \tag{9}$$

From Eq. (9), CTC can be calculated in the spatial domain as $c_{klm}(\mathbf{x}_1,\mathbf{x}_2)$. As shown in Fig. 3, after performing inverse fast Fourier transform (IFFT) to $c_{klm}(\mathbf{x}_1,\mathbf{x}_2)$, $C_{KLM}(\mathbf{f}_1,\mathbf{f}_2)$ can be efficiently obtained, which directly lead to fast algorithms for the CTC calculation as the time-consuming integration in Eq. (8) is avoided and replaced by the simple multiplication of $k(\mathbf{x}_1,\mathbf{x}_2)$, $l(\mathbf{x}_1,\mathbf{x}_2)$ and $m(\mathbf{x}_1,\mathbf{x}_2)$.

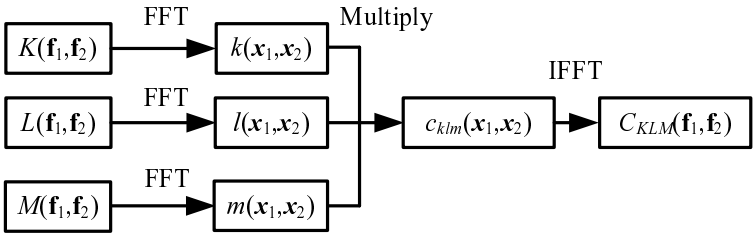

Fig. 3. Block diagram of FFT based CTC algorithm.

2.3 CTC based quadratic aberration model

According to Eq. (2) and defining $P(\mathbf{f})=\exp[-ikW_{\text{defocus}}(\mathbf{f})]$, the expression for TCC in the case that Zernike aberrations are induced can be written as:

$$\text{TCC}(\mathbf{f}_1,\mathbf{f}_2) = \int J(\mathbf{f})P(\mathbf{f}+\mathbf{f}_1)P^*(\mathbf{f}+\mathbf{f}_2)\exp\left\{-ik\left[\sum_n \text{Z}_n R_n(\mathbf{f}+\mathbf{f}_1) - \sum_m \text{Z}_m R_m(\mathbf{f}+\mathbf{f}_2)\right]\right\} d\mathbf{f}. \tag{10}$$

Applying the Taylor series expansion of the exponential function, the TCC in Eq. (10) can be decomposed up to quadratic terms as a TCC quadratic approximation:

$$\text{TCC}(\mathbf{f}_1,\mathbf{f}_2) \approx T_0(\mathbf{f}_1,\mathbf{f}_2) + T_1(\mathbf{f}_1,\mathbf{f}_2) + T_2(\mathbf{f}_1,\mathbf{f}_2), \tag{11}$$

where $T_0(\mathbf{f}_1,\mathbf{f}_2)$, $T_1(\mathbf{f}_1,\mathbf{f}_2)$ and $T_2(\mathbf{f}_1,\mathbf{f}_2)$ represent the unaberrated TCC, linearly aberrated TCC and quadratically aberrated TCC, respectively. $T_1(\mathbf{f}_1,\mathbf{f}_2)$ and $T_2(\mathbf{f}_1,\mathbf{f}_2)$ can be further decomposed into $T_{\text{lin}}^{(n)}(\mathbf{f}_1,\mathbf{f}_2)$ and $T_{\text{quad}}^{(n,m)}(\mathbf{f}_1,\mathbf{f}_2)$ with a set of input Zerinke coefficients.

$$\text{TCC}(\mathbf{f}_1,\mathbf{f}_2) = T_0(\mathbf{f}_1,\mathbf{f}_2) + \text{Z}_n\sum_n T_{\text{lin}}^{(n)}(\mathbf{f}_1,\mathbf{f}_2) + \text{Z}_n\text{Z}_m\sum_n\sum_m T_{\text{quad}}^{(n,m)}(\mathbf{f}_1,\mathbf{f}_2). \tag{12}$$

Here, $T_{\text{lin}}^{(n)}(\mathbf{f}_1,\mathbf{f}_2)$ and $T_{\text{quad}}^{(n,m)}(\mathbf{f}_1,\mathbf{f}_2)$ are linearly aberrated TCC and quadratically aberrated TCC based on individual Zernike aberrations. Each term of $T_0(\mathbf{f}_1,\mathbf{f}_2)$, $T_{\text{lin}}^{(n)}(\mathbf{f}_1,\mathbf{f}_2)$ and $T_{\text{quad}}^{(n,m)}(\mathbf{f}_1,\mathbf{f}_2)$ can be represented as a weighted sum of several CTCs:

$$T_0(\mathbf{f}_1,\mathbf{f}_2) = C_{0,0;0,0}(\mathbf{f}_1,\mathbf{f}_2), \tag{13}$$

$$T_{\text{lin}}^{(n)}(\mathbf{f}_1,\mathbf{f}_2) = -ik\left[C_{n,0;0,0}(\mathbf{f}_1,\mathbf{f}_2) - C_{0,0;n,0}(\mathbf{f}_1,\mathbf{f}_2)\right], \tag{14}$$

$$T_{\text{quad}}^{(n,m)}(\mathbf{f}_1,\mathbf{f}_2) = -\frac{1}{2}k^2\left[C_{n,m;0,0}(\mathbf{f}_1,\mathbf{f}_2) - C_{n,0;m,0}(\mathbf{f}_1,\mathbf{f}_2) - C_{m,0;n,0}(\mathbf{f}_1,\mathbf{f}_2) + C_{0,0;n,m}(\mathbf{f}_1,\mathbf{f}_2)\right], \tag{15}$$

where $C_{k,l;m,n}(\mathbf{f}_1,\mathbf{f}_2)$ is a special CTC of the following notation with defining $R_0(\mathbf{f})=1$:

$$C_{k,l;m,n}(\mathbf{f}_1,\mathbf{f}_2) = \int J(\mathbf{f})\left\{P(\mathbf{f}+\mathbf{f}_1)\left[R_k(\mathbf{f}+\mathbf{f}_1)\cdot R_l(\mathbf{f}+\mathbf{f}_1)\right]\right\}\left\{P^*(\mathbf{f}+\mathbf{f}_2)\left[R_m(\mathbf{f}+\mathbf{f}_2)\cdot R_n(\mathbf{f}+\mathbf{f}_2)\right]\right\} d\mathbf{f}. \tag{16}$$

Consequently, substituting Eq. (12) into Eq. (1), the total image intensity can be decomposed and represented as a quadratic aberration model in the following formulations:

$$I(\mathbf{x}) \approx I_0(\mathbf{x}) + I_1(\mathbf{x}) + I_2(\mathbf{x}) = I_0(\mathbf{x}) + \sum_n Z_n I_{\text{lin}}^{(n)}(\mathbf{x}) + \sum_n \sum_m Z_n Z_m I_{\text{quad}}^{(n,m)}(\mathbf{x}), \tag{17}$$

where $I_0(\mathbf{x})$ is called the aberration-free intensity; $I_1(\mathbf{x})$ and $I_2(\mathbf{x})$ displays the aberration-induced intensity distributions of linear and quadratic terms, respectively. Similar to the $T_1(\mathbf{f}_1,\mathbf{f}_2)$ and $T_2(\mathbf{f}_1,\mathbf{f}_2)$, $I_1(\mathbf{x})$ and $I_2(\mathbf{x})$ can be decomposed into $I_{\text{lin}}^{(n)}(\mathbf{x})$ and $I_{\text{quad}}^{(n,m)}(\mathbf{x})$ multiplying by the corresponding Zerinke coefficients. Thus the $I_{\text{lin}}^{(n)}(\mathbf{f}_1,\mathbf{f}_2)$ and $I_{\text{quad}}^{(n,m)}(\mathbf{f}_1,\mathbf{f}_2)$ represent the linearly and quadratically aberrated aerial image based on individual Zernike aberrations. The $I_0(\mathbf{x})$, $I_{\text{lin}}^{(n)}(\mathbf{x})$ and $I_{\text{quad}}^{(n,m)}(\mathbf{x})$ can be directly calculated from $T_0(\mathbf{f}_1,\mathbf{f}_2)$, $T_{\text{lin}}^{(n)}(\mathbf{f}_1,\mathbf{f}_2)$ and $T_{\text{quad}}^{(n,m)}(\mathbf{f}_1,\mathbf{f}_2)$ by the formulations of

$$I_0(\mathbf{x}) = \iint O(\mathbf{f}_1) O^*(\mathbf{f}_2) T_0(\mathbf{f}_1,\mathbf{f}_2) \exp\left[-2\pi i(\mathbf{f}_1 - \mathbf{f}_2)\square\mathbf{x}\right] d\mathbf{f}_1 d\mathbf{f}_2, \tag{18}$$

$$I_{\text{lin}}^{(n)}(\mathbf{x}) = \iint O(\mathbf{f}_1) O^*(\mathbf{f}_2) T_{\text{lin}}^{(n)}(\mathbf{f}_1,\mathbf{f}_2) \exp\left[-2\pi i(\mathbf{f}_1 - \mathbf{f}_2)\square\mathbf{x}\right] d\mathbf{f}_1 d\mathbf{f}_2, \tag{19}$$

$$I_{\text{quad}}^{(n,m)}(\mathbf{x}) = \iint O(\mathbf{f}_1) O^*(\mathbf{f}_2) T_{\text{quad}}^{(n,m)} \exp\left[-2\pi i(\mathbf{f}_1 - \mathbf{f}_2)\square\mathbf{x}\right] d\mathbf{f}_1 d\mathbf{f}_2. \tag{20}$$

3. SIMULATION

3.1 Simulation of TCC quadratic approximation

We model a 0.75 NA imaging system operating at λ=193nm and defocus=0nm with a coherence factor of 0.70 in Matlab. Since each CTC and TCC are both represented by four-dimensional matrices in Cartesian coordinates (f, g; f', g'), the cross-sections of the corresponding CTC and TCC can be depicted by a matrix slice which is a two-dimensional matrices in Cartesian coordinates (f, g) with considering f'=0 and g'=0. Figure 4 depicts an example of decomposing TCC(f, g) into the unaberrated term $T_0(f, g)$, linearly term $T_1(f, g)$ and quadratic term $T_2(f, g)$ under the input an individual Zernike coefficient Z_7=0.1λ. The $e(f, g)$ is defined as a residual TCC calculated by $e(f, g)$=TCC(f, g)-[$T_0(f, g)$+$T_1(f, g)$+$T_2(f, g)$].

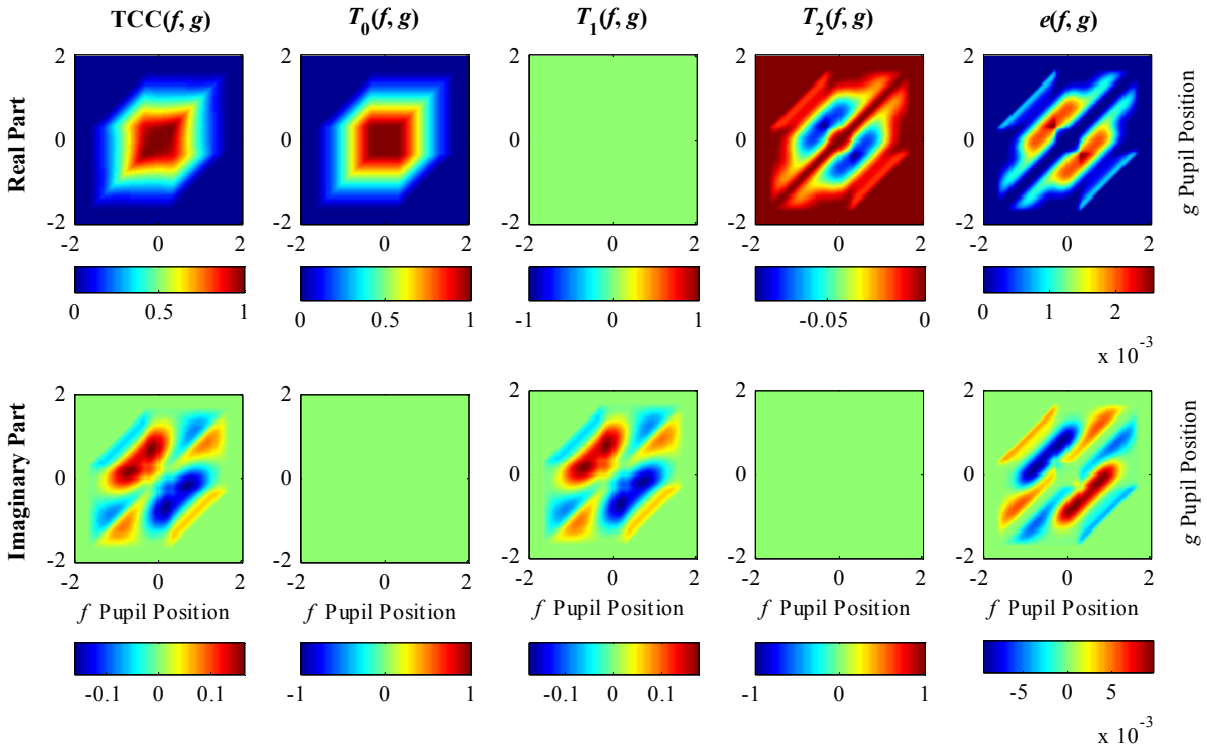

Fig. 4. An example of decomposing TCC(f, g) into the unaberrated term $T_0(f, g)$, linearly aberrated term $T_1(f, g)$ and quadratically aberrated term $T_2(f_1, f_2)$ under the input Zernike coefficient Z_7=0.1λ.

From Fig. 4, the TCC(f, g) is a complex value due to the fact that the aberration $W(\mathbf{f})$ itself is real but its exponential function term for phase change is complex in Equation (10). Because the defocus=0nm in the simulation, the $C_{k,l;m,n}(\mathbf{f}_1,\mathbf{f}_2)$ obtained from Eq. (16) keeps a real value. Determined by Eqs. (11) to (15), The linear term $T_1(f, g)$ and quadratic term $T_2(f, g)$ thus become pure imaginary and real values, respectively. It is also observed that both the real part and imaginary part of $e(f, g)$ are on the same order of 10^{-3}, which confirms that the quadratic term $T_2(f, g)$ plays the same important role in the TCC approximation as the linear term $T_1(f, g)$ plays. Considering individual aberration in current lithographic projection lens is typically less than 0.1λ, the TCC quadratic approximation will provide an efficient approach in the TCC modeling with a high accuracy.

Figure 5 illustrates an result of calculating CTCs for $T_{\text{lin}}^{(7)}(f, g)$ which multiplying by Z_7 equals to the linear term $T_1(f, g)$ in Fig. 4. Figure 6 represents the CTCs for $T_{\text{quad}}^{(7,7)}(f, g)$ which multiplying by square Z_7 equals to the quadratic term $T_2(f, g)$ shown in Fig. 4. It is interesting to note that the pairs of CTCs, such as [$C_{7,0;0,0}(f, g)$, $C_{0,0;7,0}(f, g)$], [$C_{7,7;0,0}(f, g)$, $C_{0,0;7,7}(f, g)$], and [$C_{7,0;7,0}(f, g)$, $C_{7,0;7,0}(f, g)$] are exactly the same but the coordinates (f, g) are exchanged with each other. This is due to the mathematically property of CTCs as expected in Equation (16). Therefore, for the purpose of fast calculation and simulation, we need to calculate only half of the CTCs to establish the TCC quadratic approximation.

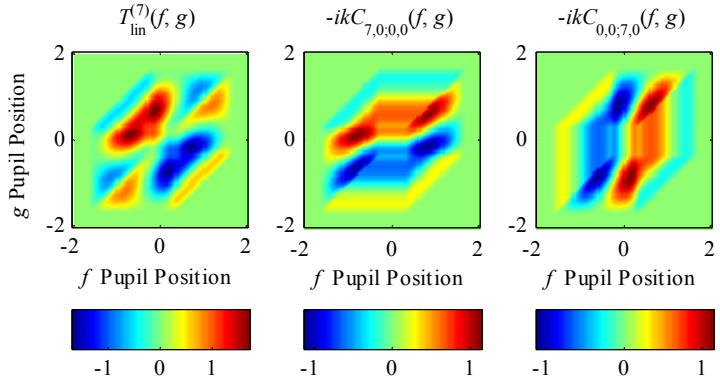

Fig. 5. Representation of the linearly aberrated TCC term $T_{\text{lin}}^{(7)}(f_1, f_2)$ as a sum of weighted CTCs.

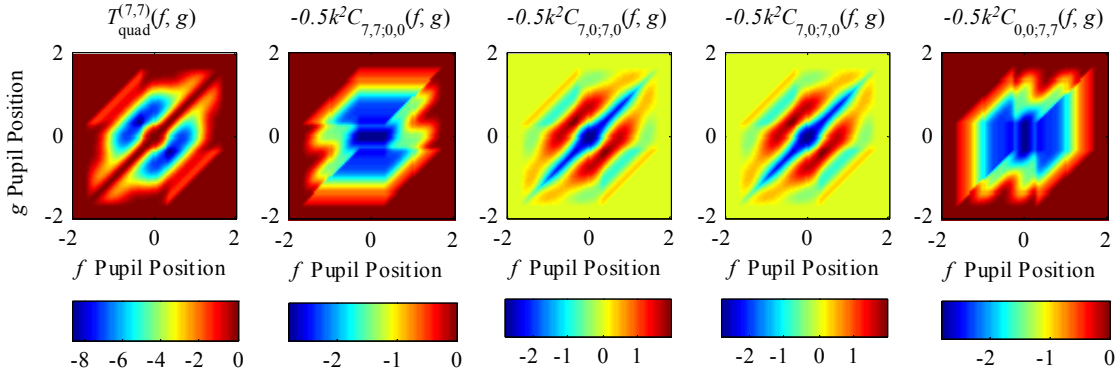

Fig. 6. Representation of the quadratically aberrated TCC term $T_{\text{quad}}^{(7,7)}(f, g)$ as a sum of weighted CTCs.

3.2 Simulation of CTC based quadratic aberration model

To simulate the CTC based quadratic aberration model, we set the imaging system operating at λ=193nm and NA=0.75 with a coherence factor of 0.35 and defocus of 100nm. Both the one-dimensional binary grating (pitch=1000nm, opening width=100nm) and alternating phase shift grating (pitch=1000nm, opening width=500nm) are utilized as input mask patterns for example. The total image intensity can be decomposed and represented as a quadratic aberration model which is expressed by the sum of the aberration-free intensity $I_0(\mathbf{x})$, linear intensity term $I_1(\mathbf{x})$ and quadratic intensity term $I_2(\mathbf{x})$. The error of the quadratic aberration model is introduced as $e(\mathbf{x})$ with the expression of $e(\mathbf{x})=I(\mathbf{x})-[I_0(\mathbf{x})+I_1(\mathbf{x})+I_2(\mathbf{x})]$.

Figure 7 shows the simulation results of the binary grating and alternating phase shift grating under the input individual Zernike coefficient Z_9=0.1λ which is a even type aberration. From Fig. 7, it is noted that both the linear term $I_1(x)$ and quadratic term $I_2(x)$ contribute to a symmetrical effect on the image intensity distribution, as the aberration-free intensity $I_0(x)$ is symmetrical about x=0. The model error $e(x)$ thus shows a small amount of and a symmetrical intensity distribution on the order of 10^{-3}, when the maximum value of $I_0(x)$ is normalized to 1.

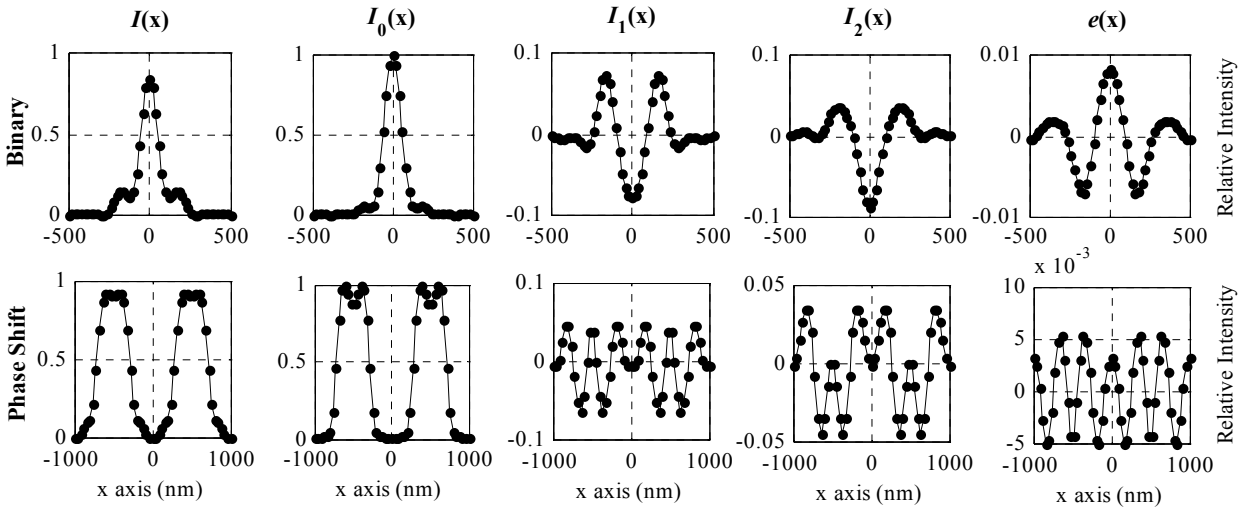

Fig. 7. Simulation result of the quadratic aberration model for the binary grating and alternating phase shift grating under the input parameters: NA=0.75, λ=193nm, Z_9=0.1λ, σ=0.35, defocus=100nm.

Figure 8 illustrates the simulation results of the binary grating and alternating phase shift grating under the input individual Zernike coefficient Z_7=0.1λ which is a odd type aberration. From Fig. 8, it is observed that the linear term $I_1(x)$ shows an asymmetrical effect on the image intensity distribution, different from that in Fig. 7. The quadratic term $I_2(x)$ create a symmetrical intensity distribution similar to that shown in Fig. 7. The model error $e(x)$ also keeps a small value on the order of 10^{-3}, which demonstrates that the quadratic aberration model achieves a high accuracy in the aerial image intensity approximation.

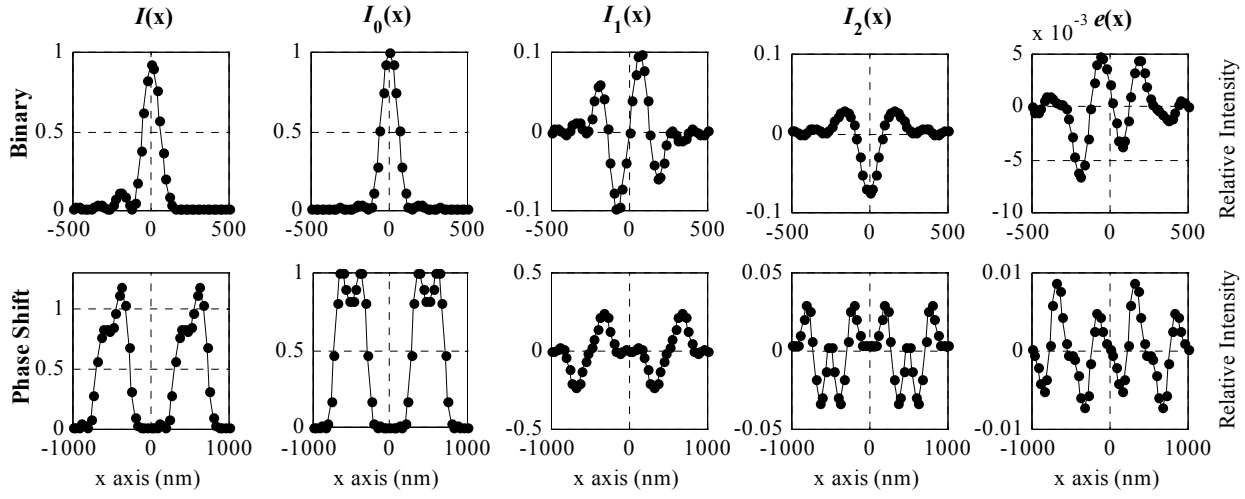

Fig. 8. Simulation result of the quadratic aberration model for the binary grating and alternating phase shift grating under the input parameters: NA=0.75, λ=193nm, Z_7=0.1λ, σ=0.35, defocus=100nm.

Except one-dimensional masks with multiple pitches and orientations are input for simulations, a contact cross pattern are designed as a two-dimensional mask for simulating the quadratic aerial image model. Figure 9 depicts the calculation result based on the contact cross pattern with setting parameters of NA=0.75, λ=193nm, Z_7=0.1λ, σ=0.70 and

defocus=0nm. From Fig. 9, the linear term $I_1(x, y)$ appears asymmetrical about x axis but symmetrical about y axis, while the aberration-free intensity $I_0(x, y)$ is symmetrical about $(x, y)=(0,0)$. This effect is due to the asymmetric property of Z_7 aberration about f axis on the pupil plane. The quadratic term $I_2(x, y)$ contributes a symmetric effect on the image intensity distribution, similar to the one dimensional symmetric property of $I_2(x)$ shown in Fig. 9. The one dimensional intensity distributions can be thus considered as a cross section (y=0) of the two dimensional intensity distributions. From this observation and lots of other simulation results for binary and phase shift masks with multiple pitches and orientations, it is found that the proposed CTC based quadratic aberration model is suitable and efficient for one/two-dimensional aerial image approximation with a high accuracy.

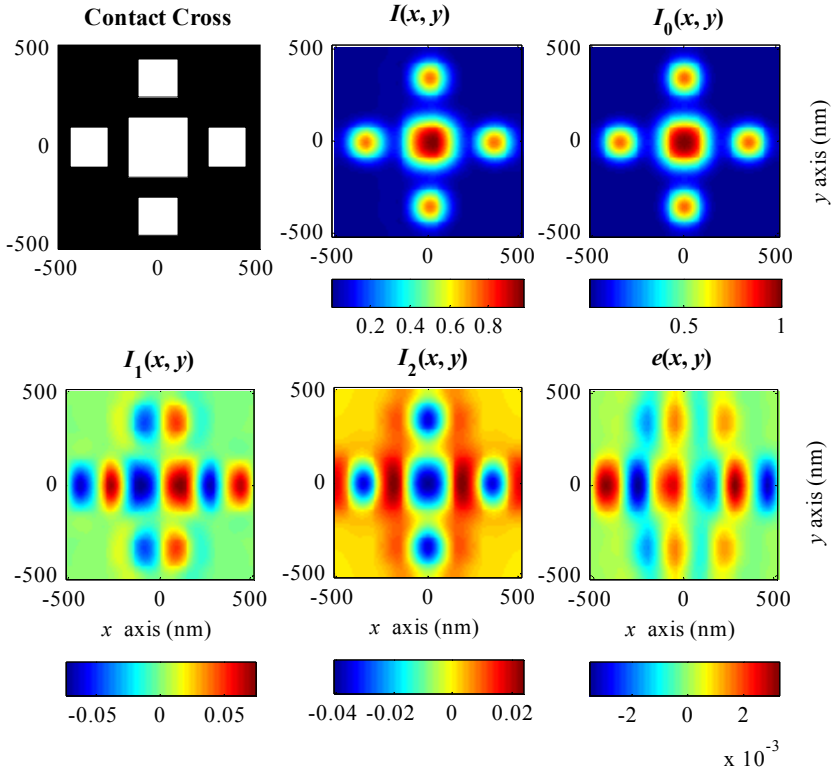

Fig. 9. Simulation result of the quadratic aberration model for the contact cross pattern under the input parameters: NA=0.75, λ=193nm, Z_9=0.1λ, σ=0.70, defocus=0nm.

4. CONCLUSIONS

We propose a CTC based method suitable for fast calculation and evaluation of quadratic aberration model in partially coherent imaging systems. By further investigating the Hopkins' imaging theory, a TCC quadratic approximation is proposed for characterizing TCC up to the quadratically aberrated term. A quadratic aberration model is subsequently established for aerial image calculation and decomposition, based on the TCC quadratic approximation. Each term in the TCC quadratic approximation can be represented as a weighted sum of several CTCs. Due to the fast algorithm for calculating CTCs, the TCC quadratic approximation and the quadratic aerial image model can be efficiently obtained. Simulations were performed by the proposed CTC based algorithm with different input Zernike aberrations for binary and phase shift masks with multiple pitches and orientations, which demonstrate that the proposed approach is not only accurate but also efficient for revealing the influence of different Zernike orders on aerial image intensity distributions under partially coherent illumination. It is expected that this method will have applications in the robust OPC and inverse mask design with aberrations taking into account. It will also have applications in the aerial image based aberration analysis and metrology.

ACKNOWLEDGMENT

This work was supported by National Natural Science Foundation of China (Grant No. 91023032, 51005091) and Fundamental Research Funds for the Central Universities of China (Grant No. 2010ZD004). The authors would like to thank National Engineering Research Center for Lithographic Equipment of China for supporting this work.

REFERENCES

[1] Smith, B. W. and Schlief, R., "Understanding lens aberration and influences to lithographic imaging," Proc. SPIE **4000**, 294-306 (2000).
[2] Liu, W., Liu, S. Y., Zhou, T. T., and Wang, L. J., "Aerial image based technique for measurement of lens aberrations up to 37th Zernike coefficient in lithographic tools under partial coherent illumination," Opt. Express **17**, 19278-19291 (2009).
[3] Liu, W., Liu, S. Y., Shi, T. L., and Tang, Z. R., "Generalized formulations for aerial image based lens aberration metrology in lithographic tools with arbitrarily shaped illumination sources," Opt. Express **18**, 20096-20104 (2010).
[4] Zernike, F., "Beugungstheorie des Schneidenverfahrens und seiner verbesserten form, der Phasenkontrastmethode," Physica **1**, 689-704 (1934).
[5] Wang, F., Wang, X. Z., and Ma, M. Y., "Measurement technique for in situ characterizing aberrations of projection optics in lithographic tools," Appl. Opt. **45**, 6086-6093 (2006).
[6] Peng, B., Wang, X. Z., Qiu, Z. C., and Yuan, Q. Y., "Measurement technique for characterizing odd aberration of lithographic projection optics based on dipole illumination," Opt. Communication **283**, 2309-2317 (2010).
[7] Yuan, Q. Y., Wang, X. Z., Qiu, Z. C., Wang, F., and Ma, M. Y., "Even aberration measurement of lithographic projection system based on optimized phase-shifting marks," Microelectron. Eng. **86**, 78-82 (2009).
[8] Nakashima, T., Higashi, K., and Hirukawa, S., "Impact of Zernike cross-term on linewidth control," Proc. SPIE **4691**, 33-43 (2002).
[9] Saleh, B. E. A., "Optical bilinear transforms," Opt. Acta **26**, 777-799 (1979).
[10] Van der Laan, H., Dierichs, M., Van Greevenbroek, H., McCoo, E., Stoffels, F., Pongers, R., and Willekers, R., "Aerial image measurement methods for fast aberration setup and illumination pupil verification," Proc. SPIE **4346**, 394-407 (2001).
[11] Flagello, D. G., Klerk, J., Davies, G., and Rogoff, R., "Towards a comprehensive control of full-field image quality in optical photolithography," Proc. SPIE **3051**, 672-685 (1997).
[12] Nakashima, T., Slonaker, S. D., Kudo, T., and Hirukawa, S., "Evaluation of Zernike sensitivity method for CD distribution," Proc. SPIE **5040**, 1600-1610 (2003).
[13] Zavyalova, L., Bourov, A., and Smith, B. W., "Automated aberration extraction using phase wheel targets," Proc. SPIE **5754**, 1728-1737 (2005).
[14] Zavyalova, L. V., Smith, B. W., Bourov, A., Zhang, G., Vellanki, V., Reynolds, P., and Flagello, D. G., "Practical approach to full-field wavefront aberration measurement using phase wheel targets," Proc. SPIE **6154**, 61540Y (2006).
[15] Hopkins, H. H., "On the diffraction theory of optical images," Proc. R. Soc. A **217**, 408-432 (1953).
[16] Lohmann, A. W. and Wirnitzer, B., "Triple correlations," Proc. IEEE **72**, 889-901 (1984).